

DNA supercoiling suppresses real-time PCR: a new approach to the quantification of mitochondrial DNA damage and repair

Jinsong Chen¹, Fred F. Kadlubar² and Junjian Z. Chen^{1,*}

¹Department of Surgery, Division of Urology, McGill University Health Centre and Research Institute, Montreal, Quebec H3G 1A4, Canada and ²Department of Epidemiology, University of Arkansas for Medical Sciences, Little Rock, AR 72205, USA

Received September 15, 2006; Revised November 26, 2006; Accepted December 27, 2006

ABSTRACT

As a gold standard for quantification of starting amounts of nucleic acids, real-time PCR is increasingly used in quantitative analysis of mtDNA copy number in medical research. Using supercoiled plasmid DNA and mtDNA modified both *in vitro* and in cancer cells, we demonstrated that conformational changes in supercoiled DNA have profound influence on real-time PCR quantification. We showed that real-time PCR signal is a positive function of the relaxed forms (open circular and/or linear) rather than the supercoiled form of DNA, and that the conformation transitions mediated by DNA strand breaks are the main basis for sensitive detection of the relaxed DNA. This new finding was then used for sensitive detection of structure-mediated mtDNA damage and repair in stressed cancer cells, and for accurate quantification of total mtDNA copy number when all supercoiled DNA is converted into the relaxed forms using a prior heat-denaturation step. The new approach revealed a dynamic mtDNA response to oxidative stress in prostate cancer cells, which involves not only early structural damage and repair but also sustained copy number reduction induced by hydrogen peroxide. Finally, the supercoiling effect should raise caution in any DNA quantification using real-time PCR.

INTRODUCTION

Alteration in human mitochondrial function is proposed to play a central role in metabolic and degenerative diseases, aging and cancer (1). Mitochondrial DNA (mtDNA) has not only been studied extensively in degenerative diseases and aging, but also drawn increasing

attention in cancer research (2–4). The human mitochondrial genome, consisting of 16 569 base pairs, is haploid, circular DNA that is semi-autonomously maintained in mitochondria, and exists in multiple copies in each cell. It contains a main control region and 37 genes coding for 13 polypeptides involved in the electron transport chain (ETC), 22 tRNAs and 2 rRNAs necessary for synthesis of the polypeptides (5,6). The ETC that located in the inner membrane of mitochondria not only plays an important role in cellular energy production through oxidative phosphorylation, but also is a major source of reactive oxygen species (ROS) (7,8). Because of its close proximity to the ETC, mtDNA is prone to oxidative injury, which is likely responsible for frequent changes in mitochondrial gene expression and somatic mutations detected in many human cancers (9–13). Early studies on 8-oxoguanine (8-oxoG), the most common oxidative base lesion, suggest that mtDNA is more susceptible to damage than nuclear DNA (14–17). Recent studies using semi-quantitative long PCR revealed more extensive and persistent oxidative mtDNA damage as compared to nuclear DNA (18,19).

Maintenance of the structural integrity of the mitochondrial genome is essential to normal mitochondrial function. In mammalian cells, the mature closed-circular mtDNA is topologically linked and assumes a supercoiled configuration with an average of 100 negatively superhelical turns (20). It has long been recognized that the negative supercoiling is the substrate for the initiation of mtDNA replication and transcription in the cell (21–23). Like other closed-circular plasmid and viral DNA, the replication requires repeated enzymatic nicking and rapid rejoining of parental molecules to relax the supercoiling (21). Thus, it is highly likely that disruption of the supercoiled conformation may have direct functional consequences in mitochondrial bioenergetics. Using the method of gel electrophoresis that detects three archetypal conformations of mtDNA, i.e. supercoiled, relaxed circular and linear forms, early studies identified that the supercoiled mtDNA is susceptible to oxidative damage

*To whom correspondence should be addressed. Tel: +1 514 934 1934 x 44601(o); Fax: +1 514 934 8261; Email: junjian.chen@mcgill.ca

(24–28). Recent evidence suggests that disruption of the supercoiled structure is associated with functional changes in animal mitochondria (29,30). Thus, the structural integrity of mtDNA may serve as a functionally relevant DNA marker to oxidative damage. However, the detection of conformational/structural damage using conventional gel electrophoresis is not quantitative and very tedious process that requires coupling of Southern blot and probe hybridization. The long PCR assay (31), on the other hand, allows quantification of mtDNA damage directly from genomic DNA, but provides little information about the structures of mtDNA. Further investigation of the structural change in mtDNA using new analytical approaches may provide a new perspective to the role of oxidative damage in aging and cancer.

Real-time PCR is a powerful technique that allows accurate quantification of starting amounts of nucleic acids during a PCR reaction and without post-PCR manipulation (32,33). It relies on a fluorescent reporter, either alone or conjugated to a probe that monitors the accumulation of double-stranded products with each successive cycle. Quantification is achieved by measuring the increase in fluorescence during the exponential phase of PCR or the threshold cycle (Ct) of PCR. Because of its high sensitivity and wide dynamic range, real-time PCR becomes the most sensitive method for the quantification of gene expression when coupled with reverse transcription (34). It is also increasingly used for quantification of mtDNA content or specific mutant species in clinical and toxicity studies (35–40). In practice, the relative mtDNA content is measured as the ratio of mtDNA versus a reference nuclear gene. However, the vastly different structural complexities of mitochondrial and genomic DNA make real-time PCR quantification difficult. To our best knowledge, the effect of mtDNA conformations on real-time PCR quantification has not been reported. Since mtDNA exists as a mixture of supercoiled, relaxed and linear forms both in the cell and in the extracted form, it is not clear if the supercoiled form has the same efficiency as the relaxed forms in real-time PCR amplification. In this study, we investigated the effect of conformational structures of mtDNA on real-time PCR quantification using plasmid DNA as a model molecule and mtDNA modified both *in vitro* and in cancer cells. We demonstrated a dramatic increase or decrease in real-time PCR quantification when supercoiled DNA was converted into relaxed forms. Moreover, the extent of structural changes could be accurately quantified based on the Ct value. A sensitive new approach was described for simultaneous detection of both copy number change and structure-mediated damage and repair in mtDNA of cancer cells.

MATERIALS AND METHODS

Cell culture

LNCaP, an androgen responsive prostate cancer cell with a functional p53 gene, was purchased from the ATCC (Manassas, VA). LNCaP cells were grown in RPMI-1640 medium containing 10% FBS (Gibco, Grand Island, NY) on 1% Poly-L-Lysine solution

(Sigma-Aldrich, St Louis, MO) coated dishes and maintained at 37°C in an incubator supplemented with 5% CO₂.

DNA preparation

Total genomic DNA containing nuclear and mtDNA from LNCaP cells was isolated using the Qiagen Genomic-tip kit (Valencia, CA). Minor modifications were made to the recommended protocol so that mtDNA was always isolated together with nuclear DNA. The Qiagen procedure is an ion-exchange system and, unlike phenol-based methods, does not oxidize purines during isolation (41). Supercoiled pBR322 DNA was purchased from Invitrogen (Carlsbad, CA). Both plasmid and genomic DNA was precisely quantified using a two-step procedure using the PicoGreen dsDNA Quantification Kit (Molecular Probes, Eugene, OR).

Enzymatic digestion of plasmid and total genomic DNA

pBR322 plasmid DNA was digested with enzymes that relax the supercoiled form (Figure 1A). EcoR I (New England Biolabs, Ipswich, MA) that has a single restriction site in pBR322 DNA was used to generate its linear forms. N.BstNB1 (New England Biolabs) that has two nicking sites in pBR322 DNA was used to generate the nicked circular form. Topoisomerase I (Invitrogen) relaxes negative supercoiling and was used to generate relaxed closed-circular topoisomers of plasmid DNA. Total genomic DNA from LNCaP was also digested with EcoR1 to linearize mtDNA. Digested plasmid and total genomic DNA was recovered by ethanol precipitation and quantified using the PicoGreen dsDNA Quantification Kit.

Ferrous iron (Fe⁺⁺)-induced damage in plasmid and total genomic DNA *in vitro*

1 M FeSO₄ (Fisher) stock solution was freshly prepared in 5 mM H₂SO₄ to prevent oxidation (Fisher, Hampton, NH) (42). To induce structural damage in plasmid DNA, 1.5 μg of each pBR322 DNA was treated with 0, 10, 50 and 100 μM FeSO₄ with or without the presence of 100 mM D-mannitol (Sigma), a scavenger of hydroxyl radical (43). All treatments were carried out in 100 mM potassium phosphate buffer (pH 7) for 15 min at room temperature. Treated DNA in the presence of 200 mM NaCl and 20 μg glycogen was recovered with addition of the same volume of isopropanol. To induce DNA damage, 2 μg of each total genomic DNA was exposed to 0, 10, 100 μM FeSO₄, and 100 μM FeSO₄ plus 100 mM D-mannitol under the same condition used for plasmid DNA. Total genomic DNA was immediately recovered by isopropanol precipitation after 15-min exposure. Duplicate treatments were performed for both plasmid and total genomic DNA. The recovered DNA was quantified using the two-step PicoGreen dsDNA Quantification method.

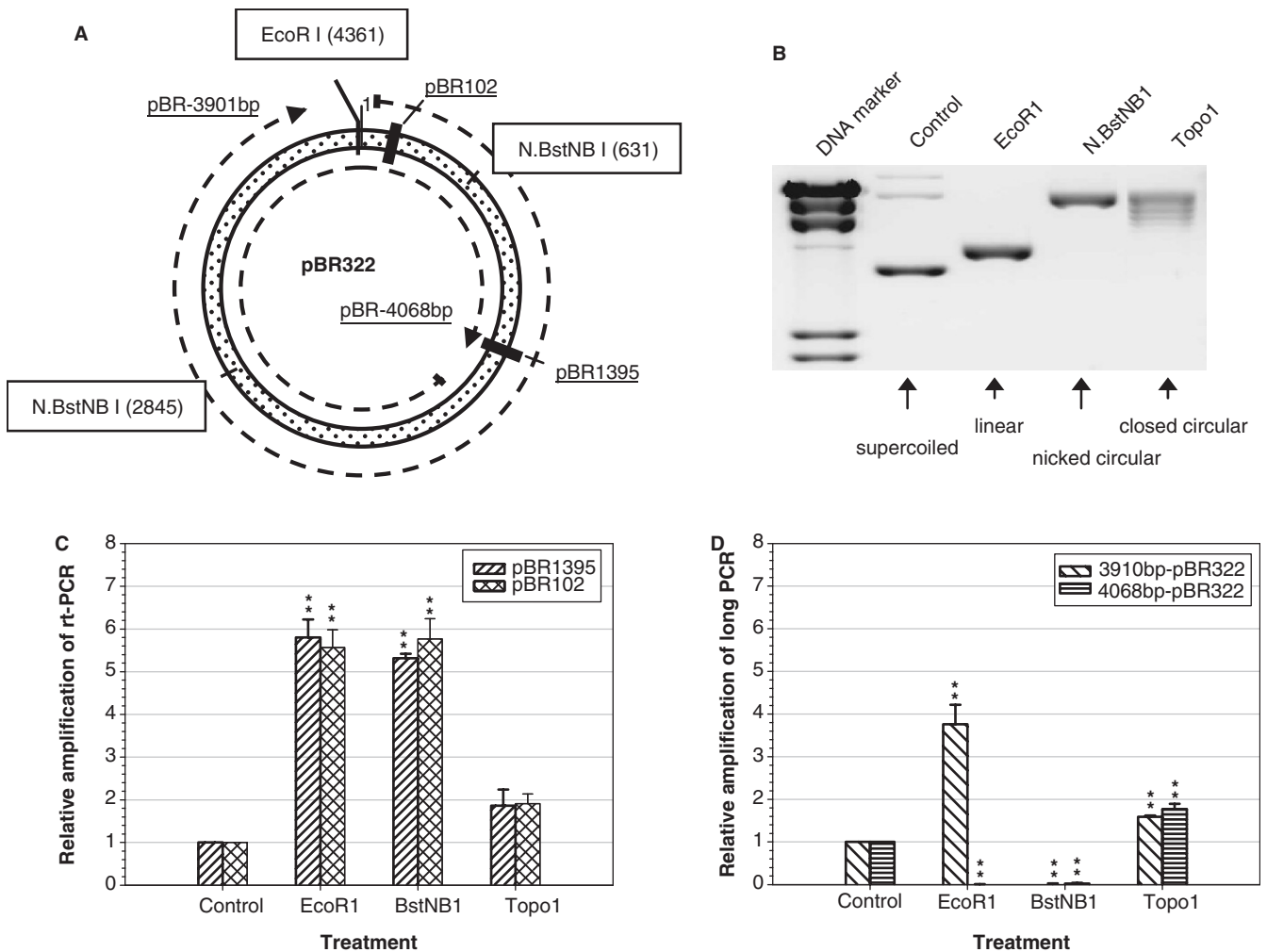


Figure 1. The effect of supercoiling of plasmid DNA on real-time PCR. Supercoiled plasmid DNA, pBR322 was treated with EcoR1, N.BstNB1 and Topoisomerase I to generate linear, nicked circular and closed circular forms, respectively, and analyzed using gel electrophoresis and quantitative PCR assays. (A) Distribution of enzymes' cutting sites and DNA markers for real-time PCR (rt-PCR, black bars) and long PCR (dashed lines) assays. (B) Electrophoresis of treated plasmid DNA in 1% agarose gel. DNA bands were visualized by ethidium bromide staining after electrophoresis. (C) The effect of supercoiling on real-time PCR. Two short DNA markers (pBR102 and pBR1395) were analyzed for each samples using SYBR green dye. The relative amplification of real-time PCR was expressed as $2^{\Delta Ct}$. (D) Detection of blocking lesions using long PCR. Two long DNA markers (pBR-3901 bp and pBR-4068 bp) were amplified to detect the blocking effects of double and single strand breaks in plasmid DNA. The relative amplification of long PCR was expressed as A_D/A_O . The 3901-bp fragment excluded the EcoR1 site but flanked two nicking sites of N.BstNB1, while the 4068-bp fragment covered all three sites. Data from duplicate treatments were pooled and analyzed using the one-way analysis of variance in the Prism program (** $P < 0.01$).

Hydrogen peroxide (H₂O₂)-induced DNA damage in LNCaP cells

LNCaP cells of $2-3 \times 10^6$ were seeded in each 100-mm dish containing 10 ml complete RPMI-1640 medium 48 h before treatment. A working solution of 1 M H₂O₂ was freshly prepared in PBS using 50% stock solution (Fisher) and placed on ice. For exposure experiments, duplicate dishes of LNCaP cells were treated with 120 and 240 μ M H₂O₂ in serum-free medium for 15 and 60 min, respectively. For recovery experiment, LNCaP cells were first treated with 120 and 240 μ M H₂O₂ in serum-free medium for 60 min, then allowed to recover in fresh complete medium for 2 and 24 h. LNCaP cells in control dishes were mock treated in serum-free medium for

60 min, and collected immediately or after a 24-h culture in complete medium. LNCaP cells were collected using trypsin digestion. The cell pellets were washed once in PBS solution and stored in 1.5 ml micro-centrifuge tubes at -80°C until analysis.

Agarose gel electrophoresis of plasmid DNA

pBR322 DNA of 80 ng treated either by enzymes or ferrous iron were electrophoresed at 30–40 V for 12–16 h in 1% agarose gel and 1X TBE buffer. The agarose gel was stained in ethidium bromide solution after electrophoresis and visualized using an automated gel documentation system (Syngene, Frederick, MD).

Real-time PCR analysis of plasmid and total genomic DNA

The MyiQ real-time PCR system (Bio-Rad, Hercules, CA) was used for analysis. Multiple mtDNA markers distributed around the genome and two nuclear DNA markers were used for real-time PCR using the SYBR Green I intercalation dye. The sequence information of all the primers was listed in Table 1. Total genomic DNA of 3 and 15 ng were used for mtDNA and nuclear DNA markers, respectively, in a 50 μ l reaction containing 1X iQTM SYBR Green 1 Supermix (Bio-Rad), 3.5 mM MgCl₂, and 300 nM each of primers. Duplicate or triplicate reactions were performed for each marker in a 96-well plate using a two-step amplification program of initial denaturation at 95°C for 3 min, followed by 30–35 cycles of 95°C for 20 s and 61°C for 30 s. A melt curve analysis step was enabled at the end of the amplification, which consists of denaturation at 95°C for 1 min and re-annealing at 55°C for 1 min, followed by increasing setpoint temperature each cycle by 1°C for 40–45 cycles. Standard curves were generated from each experimental plate using serial 5-fold dilutions of untreated genomic DNA. The Ct for each reaction was calculated using the MyiQ software. Amplification efficiencies calculated according to the equation $E = 10^{(-1/\text{slope})}$ (33) ranged from 90–104% for nuclear and mtDNA markers; no unspecific amplification or primer dimer was observed in any of the markers as confirmed by the melt curve analysis (S. Figures 1 and 2 in Supplementary Data). To compensate for potential differences in E between markers, the ratio of relative expressions was computed, based on the efficiency (E) and the Ct difference (Δ) of sample versus control ($\Delta C_{t(\text{control-sample})}$), and then normalized by a nuclear reference gene, β -actin, according

to the equation (44):

$$R_{\text{target}} = \frac{(E_{\text{target}})^{\Delta C_{t(\text{control-sample})}}}{(E_{\text{ref}})^{\Delta C_{t(\text{control-sample})}}} \quad 1$$

Data from duplicate treatments were pooled and analyzed using the one-way analysis of variance in the Prism 4 software (Graphpad, San Diego, CA).

Two plasmid DNA markers were used for real-time PCR as described earlier except that 100 μ g plasmid DNA was used for each reaction (Figure 1A and Table 1). Standard curves were generated in each plate using serial dilutions of untreated plasmid DNA. The structural change in treated samples was calculated using the equation $R_c = 2^{\Delta C_t}$ (32), where R_c was the relative expression change, ΔC_t was the $C_{t(\text{control})} - C_{t(\text{sample})}$, and the E ranges from 95 to 100% (S. Figure 3 in Supplementary Data).

Quantitative long PCR assay for plasmid and total genomic DNA

Long PCR for mtDNA and nuclear DNA was performed using the GeneAmp XL PCR kit (Perkin-Elmer, Boston, MA) according to the protocol described previously (31). A 16.2-kb mtDNA fragment that amplifies more than 98% mitochondrial genome and a 13.5-kb β -globin gene were used to quantify polymerase blocking lesions in mtDNA and nuclear DNA, respectively (Table 2). For plasmid DNA analysis, two pBR322 DNA markers were designed to amplify 3901-bp and 4068-bp fragments (Figure 1A and Table 2). The long PCR amplifications were performed using the same reaction mixture as for mtDNA except that 166 μ g of pBR322 DNA was used for each amplification. A modified two-step cycling program was used for plasmid DNA markers, which consisted of initial denaturation at 94°C for 1 min, followed by 18 cycles of 94°C for 30 s and 66°C for 4.6 min. The reaction was extended for 10 min at 72°C at the last cycle. Relative amplification was calculated by normalizing the amplification of treated samples (A_D) to that

Table 1. Sequences of primers for real-time PCR

Target	Primer/location	Sequence (5'-3')
CO2 (mtDNA)	CO2F	CCCCACATTAGGCTTA AAAACAGAT
	CO2R	TATACCCCGGTCGTG TAGCGGT
D-loop (mtDNA)	DloopF	TATCTTTTGGCGGTAT GCACTTTAACAGT
	DloopR	TGATGAGATTAGTAGT ATGGGAGTGG
β -actin	ActinF	TCACCCACACTGTGCC CATCTACGA
	ActinR	CAGCGGAACCGCTCAT TGCCAATGG
β -globin	BG354F	GTGCACCTGACTCCTG AGGAGA
	BG455R	CCTTGATACCAACCTGC CCAG
pBR102 (pPB322)	pBR102F	CAGGCACCGTGTATGA AATCTA
	PBR102R	ATAGTACTGGCGATG CTGT
pBR1395 (pBR322)	pBR1395F	CAACCCTTGGCAGAACA TATCC
	pBR1395R	AACGACAGGAGCACGA TCAT

Table 2. Sequences of primers for quantitative long PCR

Target	Primer/location	Sequence (5'-3')
16.2-kb mtDNA	mt15149F	TGAGGCCAAATATCATTCTGA GGGGC
	mt14841R	TTTCATCATGCGGAGATGTTG GATGG
13.5-kb β -globin	bg48510F	CGAGTAAGAGACCATTGTGG CAG
	bg62007R	GCATGGCTTAGGAGTTGG AC
3.9-kb pBR322 (pBR-3901bp)	pBR102F	CAGGCACCGTGTATGAAAT CTA
	pBR399R	TGGATCTCAACAGCGGTAA GA
4.1kb pBR 322 (pBR-4068bp)	pBR1753F	GGCATTGACCCTGAGTGAT TT
	pBR1395R	AACGACAGGAGCACGAT CAT

of non-damaged controls (A_0). Data from duplicate treatments were pooled and analyzed using the one-way analysis of variance in the Prism 4 software (Graphpad).

RESULTS

The effect of supercoiling of plasmid DNA on real-time PCR

Supercoiled pBR322 plasmid DNA was previously shown to be a reliable standard for conformational studies of mtDNA (28). It contains an average of 30 negative supercoiled turns (45,46). Using supercoiled pBR322 DNA as a substrate, the linear, nicked circular and relaxed closed-circular forms of DNA were generated by topoisomerase or enzymatic digestion and separated by gel electrophoresis (Figure 1A and B). The conformationally changed DNA was then analyzed using real-time PCR. Using the same amount of starting template DNA and two plasmid DNA markers, real-time PCR detected near 6-fold increases in amplification of both linear and nicked circular forms as compared to the untreated supercoiled DNA, while only 2-fold increases were observed in the closed circular forms (Figure 1C). The later observation was further confirmed by reducing various amounts of supercoiled turns using Topoisomerase 1 treatment (S. Figure 4 in Supplementary Data). Thus, the negatively supercoiled DNA was a poor substrate for real-time PCR. The disruption of the negative supercoiling by strand breaks dramatically increased the efficiency of real-time PCR amplification, while relaxation of superhelical turns alone had limited effect on real-time PCR. We reasoned that the disrupted forms of plasmid DNA were more accessible for primer binding and elongation, leading to increased PCR amplification. Importantly, real-time PCR that amplifies only short amplicons did not detect DNA lesions themselves but rather their global (or distant) effects on altered DNA conformations. This was in contrast with long PCR amplification that was sensitive to blocking lesions. Using near-whole plasmid amplification, we demonstrated that both double- and single-strand breaks generated by complete EcoR1 and N.BstNB1 digestion, respectively, were strong blocking lesions for long PCR amplification (Figure 1D). However, a 4-fold increase in long PCR amplification was observed when the sole EcoR1 cutting site was located outside of a 3901-bp amplicon, suggesting that DNA strand breaks have two types of effect on long PCR amplification depending on their distribution. Interestingly, the relaxation of supercoiled turns by Topoisomerase 1 had only limited effect on long PCR, similar to that of real-time PCR.

Fe⁺⁺-induced DNA strand break and structural disruption in plasmid DNA

The dramatic effect of conformational structure on real-time PCR rendered the technique useful in detecting structure-mediated DNA damage. Ferrous iron, a transition metal that promotes hydroxyl radical production (47), was used to introduce random DNA damage to plasmid DNA, while mannitol was used as a free radical scavenger to protect DNA from Fe⁺⁺-induced hydroxyl

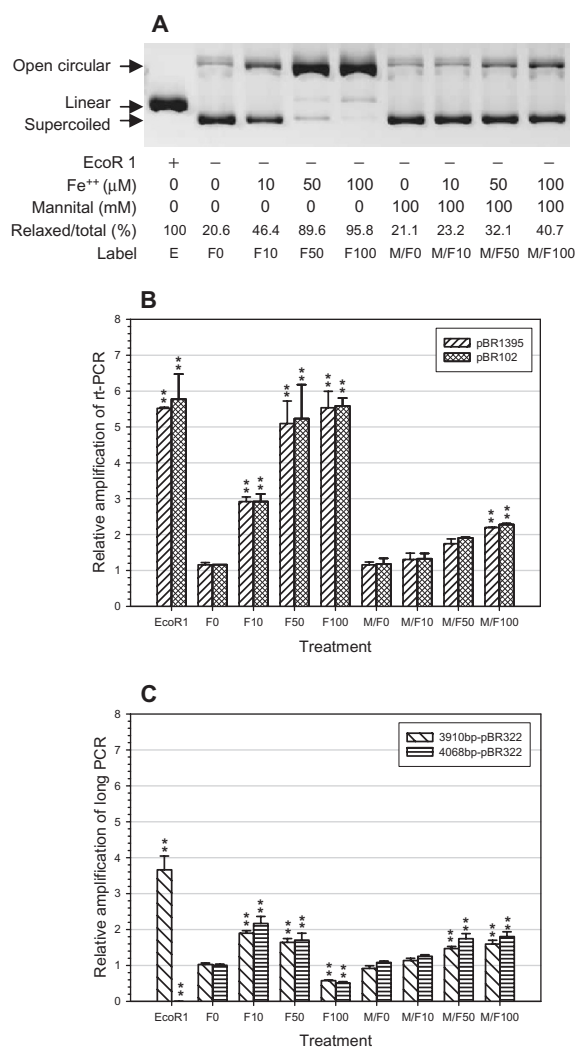


Figure 2. Fe⁺⁺-induced DNA strand breaks and structural disruption in plasmid DNA. Supercoiled pBR322 DNA was either digested with EcoR1, or treated for 15 min with various concentrations of Fe⁺⁺ with or without mannitol in 100 mM potassium phosphate buffer (pH 7.0). (A) Electrophoresis of treated plasmid DNA in 1% agarose gel. Induced changes in conformational state of plasmid DNA were visualized by ethidium bromide staining after electrophoresis. The ratio of relaxed form (nicked circular+linear) vs. total DNA was computed using the Genetools software (Beacon House). (B) Detection of structural disruption in plasmid DNA induced by Fe⁺⁺ and mannitol treatment using real-time PCR. (C) Detection of blocking lesions in plasmid DNA induced by Fe⁺⁺ and mannitol treatment using long PCR. Data from duplicate treatments were pooled and analyzed using the one-way analysis of variance in the Prism program (* $P < 0.05$; ** $P < 0.01$).

radical attack. As visualized by gel electrophoresis (Figure 2A), Fe⁺⁺ treatment alone induced a dose-dependent increase in percentage of the open circular form of plasmid DNA, indicating an accumulation of single-strand breaks. Addition of mannitol, however, dramatically reduced the formation of open circular DNA, which was consistent with the suppressing effect of hydroxyl radical scavengers on the formation of DNA strand breaks induced by transition metals (47,48). When

Fe^{++} -treated samples were analyzed using real-time PCR, the increase in real-time PCR amplification signal was positively correlated with the percentage of open circular DNA in each sample, with the maximum responses observed when most, if not all, of the supercoiled molecules were converted into the nicked circular forms as in 50 and 100 μM Fe^{++} treatments (Figure 2B). Thus, real-time PCR amplification increased as single-strand DNA breaks were introduced into an initially supercoiled DNA. Since neither the amplification signal (Figure 2B) nor the percentage of open circular DNA (Figure 2A) increased between 50 and 100 μM Fe^{++} treatments, the real-time PCR signal was more correlated with the percentage of molecules containing at least one strand break than with the number of breaks in each molecule. The accumulation of multiple DNA strand breaks in the same molecule appeared to have no additional impact on real-time PCR. On the other hand, long PCR analysis of the Fe^{++} -treated DNA revealed a very different pattern of amplification with both increased and decreased PCR products observed, depending on the concentration of Fe^{++} treatments (Figure 2C). The complicated pattern of amplification signals suggests that randomly induced DNA strand breaks also have a 2-fold effect on long PCR amplification. Perhaps, the first strand break relaxes the supercoiling and increases the amplification signal by allowing complete separation of DNA strands. All breaks reduce amplification signal by blocking fork progression. The final result is complex kinetics of signal versus break. Thus, real-time PCR was more sensitive to detect and quantify structural disruption of supercoiled DNA induced by strand breaks, especially at the low levels.

Fe^{++} -induced structural damage in mtDNA *in vitro*

Because the functional mtDNA is a negatively supercoiled form in the cell, the sensitivity of real-time PCR signal to the conformational state should illuminate structural changes in mtDNA induced by oxidative damage without necessitating the isolation of pure mtDNA. To test this, total genomic DNA isolated from prostate cancer cells was either digested by EcoRI that has a single cutting site in mtDNA or treated with Fe^{++} . Real-time PCR analysis using two mtDNA markers revealed 1.5- and 2-fold increases in mtDNA amplification when treated with 10 and 100 μM Fe^{++} (with and without mannitol), respectively, suggesting significant structural disruption in mtDNA (Figure 3A). The 2-fold increase in mtDNA amplification appeared to be the 'maximum' structural response induced in mtDNA because the same level of increase was also observed in EcoRI digested DNA. The low level of maximum response in mtDNA isolated from prostate cancer cells was in contrast to that of near 6-fold increases observed in plasmid DNA. This cannot be explained by differences in supercoiled density in two molecules. Instead, it is most likely due to a high baseline level of relaxed fraction in mtDNA (~45%) extracted from untreated cancer cells as compared to a low level of relaxed fraction in untreated plasmid DNA (~20%). On the other hand, it was expected that Fe^{++} -induced strand breaks were primarily responsible for the structural

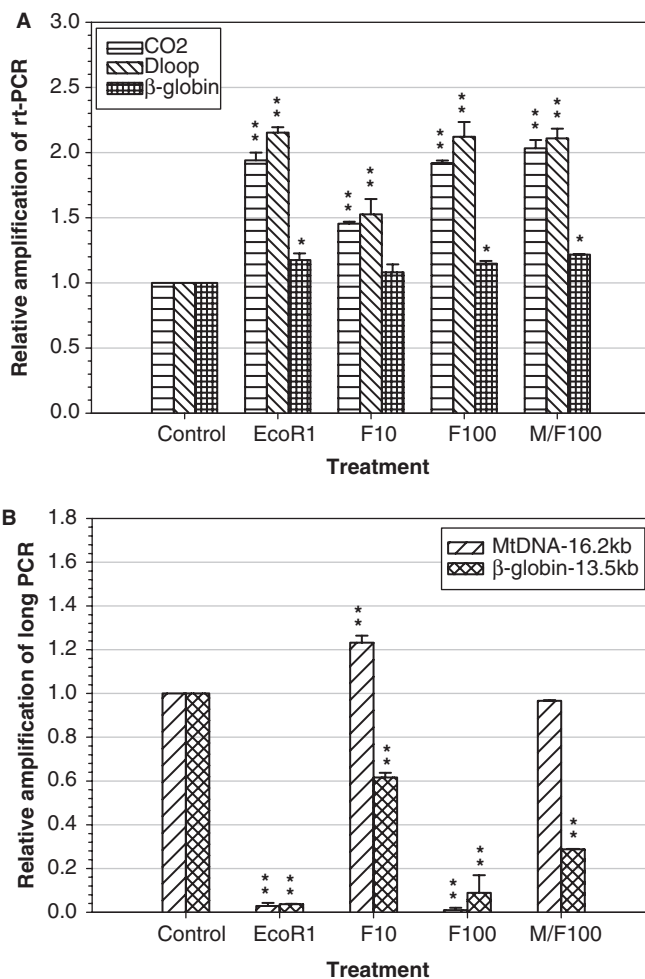


Figure 3. Fe^{++} -induced structural damage in mtDNA *in vitro*. Total genomic DNA isolated from LNCaP cells was either digested by EcoRI or treated for 15 min with 10 and 100 μM Fe^{++} with or without mannitol in 100 mM potassium phosphate buffer (pH 7.0). (A) Detection of structural damage in mtDNA induced by Fe^{++} and mannitol treatment using real-time PCR. Two mtDNA markers (CO2 and Dloop) and two nuclear DNA markers (β -actin and β -globin) were analyzed using real-time PCR. The relative amplification of mtDNA markers and β -globin was calculated by normalizing to the reference gene of β -actin according to Equation 1 (see Materials and Methods). (B) Blocking effects of Fe^{++} -induced DNA lesions in both mtDNA and nuclear DNA using long PCR. A 16.2-kb mtDNA and a 13.5-kb β -globin fragments were amplified using long PCR. The ratio of PCR amplification relative to the non-treated control was determined in both mtDNA and nuclear DNA. Data from duplicate treatments were pooled and analyzed using the one-way analysis of variance in the Prism program (* $P < 0.05$; ** $P < 0.01$).

disruption detected by real-time PCR, although addition of mannitol to the 100 μM Fe^{++} treatment failed to reduce real-time PCR amplification. Indeed, 100 μM Fe^{++} treatment completely blocked the amplification of a 16.2-kb mtDNA fragment, so did the EcoRI digestion (Figure 3B). However, the long PCR analysis was less sensitive to the detection of low levels of DNA damage (i.e. strand breaks) in mtDNA because only control levels of the 16.2-kb probe were detected in mtDNA protected with mannitol or treated with 10 μM Fe^{++} . In fact,

a slight increase in long PCR amplification above the control was evident in the low dose of Fe⁺⁺ treatment. Thus, real-time PCR was more sensitive for detecting low levels of DNA strand breaks in supercoiled mtDNA, a feature that is important in detecting physiological levels of oxidative damage in the cell. It is conceivable that a random single-strand break was sufficient to disrupt the entire supercoiled structure of the molecule, hence facilitating real-time PCR amplification of short DNA markers throughout the genome. In contrast, the disrupted mtDNA would result in a linear and a relaxed single-strand DNA that is having opposite effects on long PCR amplification. It is worth noting that nuclear DNA is less susceptible to structural change as evidenced by little changes in the ratio of β -actin versus β -globin DNA markers in real-time PCR analysis even though substantial amount of DNA strand breaks were generated in most *in vitro* treatments.

The effect of heat-denaturation on mtDNA quantification

Heat-denaturation, an essential step in both PCR amplification and real-time PCR, allows separation of two complementary DNA strands for specific primer binding. It could also introduce DNA strand breaks into supercoiled template DNA, leading to DNA degradation (49). To evaluate the effect of heat-denaturation on real-time PCR quantification of mtDNA, the same amounts of total genomic DNA from LNCaP cells were heat denatured at 95°C for increasing time periods before real-time PCR amplification. A significant increase in real-time PCR amplification was observed during the first 3 min denaturation before reaching a plateau after 4–6-min treatment (Figure 4A). Extended heat-denaturation over 6 min had no additional impact on real-time PCR of mtDNA. In contrast, β -actin DNA amplification exhibited little change within the first 6 min of treatment, but decreased slightly after 12 min (data not shown). The heat-denaturation effect on real-time PCR amplification was also observed in plasmid DNA and was accounted for by the accumulation of single-stranded molecules caused by strand breaks and denaturation (Figure 4B and C). Several practical implications could be derived from the effect of heat-denaturation on mtDNA quantification. For example, the initial heat-denaturing time in PCR amplification could have major impact on real-time PCR analysis of mtDNA content and structural changes. As demonstrated in both plasmid and mtDNA analyses earlier, real-time PCR was more efficient when acting upon relaxed from than upon supercoiled form DNA. Short initial denaturation time would better preserve the original ratios of supercoiled versus relaxed mtDNA, therefore enhancing the sensitivity for structural analysis. However, prolonged initial denaturation could convert all supercoiled DNA into its open-relaxed forms, eliminating structural effects all together. Incorporation of these two strategies could provide a simple new approach to analyze both relaxed form and total mtDNA content simultaneously using real-time PCR (see later).

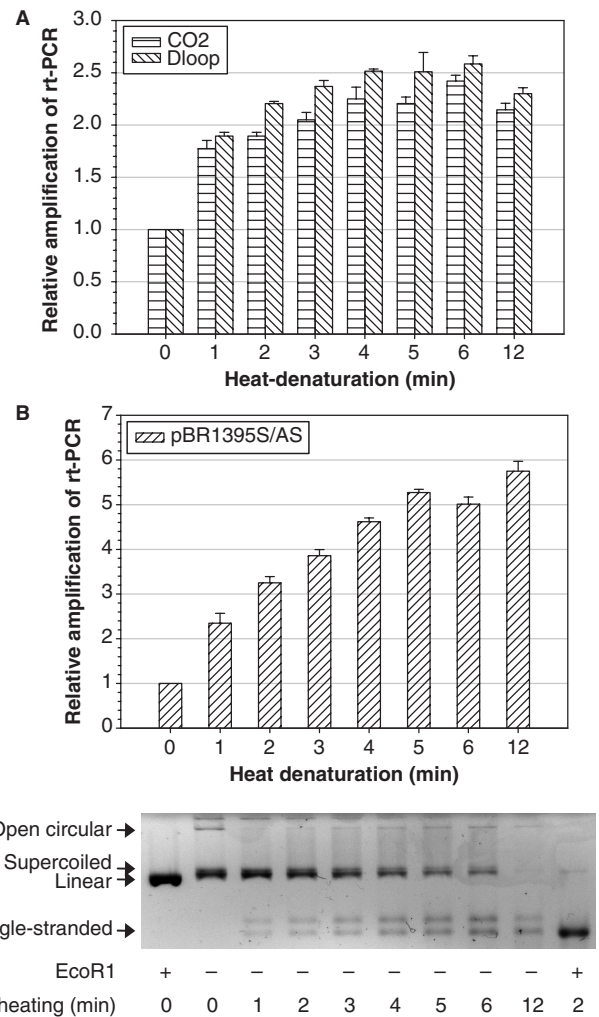


Figure 4. Effects of heat-denaturation of mtDNA on real-time PCR quantification. (A) Aliquots of 5 ng/ μ l of total genomic DNA isolated from LNCaP cells were heat-denatured at 95°C for different time periods and then used for real-time PCR amplification using two mtDNA markers and β -actin DNA marker. (B) Aliquots of 100 pg/ μ l of supercoiled pBR322 DNA were heat-denatured at 95°C and then analyzed using plasmid DNA marker pBR1395. The relative amplification of both mtDNA and plasmid DNA markers from heat-denatured templates was expressed as $2^{\Delta Ct}$, where ΔCt was $Ct_{control} - Ct_{heated}$. (C) Electrophoresis of heat-denatured plasmid DNA in 1% agarose gel. Data from duplicate treatments were pooled. Differences between untreated and treated samples were all significant ($P < 0.01$).

Simultaneous analysis of mtDNA damage, repair and copy number change in stressed prostate cancer cells

Total mtDNA consists of both supercoiled and relaxed forms both in the cell and in its extracted form. We reasoned that the supercoiled and open-relaxed forms of mtDNA reflect functional and damaged molecules, their ratio being modulated by DNA damage and repair activities in each cell. Thus, sensitive detection of the relaxed and total mtDNA from the same DNA templates should allow quantitative measurements on mtDNA damage, repair and copy number change in stressed cells. To validate this new strategy, prostate cancer cells

(LNCaP) were exposed to sub-lethal concentrations of H_2O_2 to study DNA damage at exposure and repair activity during recovery. When treated with $120 \mu M H_2O_2$, an average of 1.5- and 1.4-fold increases in mtDNA amplification were detected using two mtDNA markers after 15 and 60 min exposure, respectively (Figure 5A). The rapid increase in mtDNA amplification was unlikely due to a copy number increase, but more likely due to induction of structural damage mediated by single-strand breaks in the cell. On the other hand, the induced mtDNA amplification was reduced to the control level after 2- and 24-h recoveries, as expected from complete repair of induced mtDNA damage. The ratio of two nuclear DNA markers remained at the control level in all samples. To determine potential changes in mtDNA copy number, total genomic DNA was first heat-denatured at $95^\circ C$ for 6 min and then used for real-time PCR. Interestingly, the level of total mtDNA amplification was similar to the untreated control in all heat-denatured templates, and was higher than that of relaxed DNA in corresponding original templates (Figure 5B). Thus, the total mtDNA copy number remained unchanged during both exposure and recovery, and the increase and reduction in amplification of the relaxed mtDNA reflected primarily *in vivo* structural damage and repair. In contrast, the control level of amplification of a 16.2-kb mtDNA fragment was observed in both exposure and recovery samples (data not shown), suggesting that the long PCR analysis was not sufficiently sensitive to detect low levels of structural damage and repair in mtDNA.

When prostate cancer cells were treated with $240 \mu M H_2O_2$, an average of more than 2.1- and 1.8-fold increases in real-time PCR amplification were detected using two different mtDNA markers after 15 and 60 min exposures (Figure 6A). The dose-dependent increase in mtDNA amplification at 15-min exposure likely reflected increased levels of structural damage during early exposure. However, reduction in mtDNA amplification was evident after 60-min exposure and approached the control level in at least one of the markers during the early recovery (2hR). Interestingly, a further reduction in real-time PCR amplification of mtDNA below the control level was observed after 24 h of recovery, raising the possibility of induced changes in mtDNA copy number. Indeed, total mtDNA analysis using heat-denatured DNA templates and the CO2 marker revealed dramatic changes in total mtDNA content induced by $240 \mu M H_2O_2$ treatment (Figure 6B). As compared to the control (heated), a significant decrease in total mtDNA amplification was detectable in samples of 60 min exposure ($P < 0.05$) and two recoveries ($P < 0.01$), with nearly 2-fold reduction detected at 2 h of recovery. Moreover, the same levels of mtDNA amplification were observed in both original and heat-denatured templates from each of two exposures. Based on the simultaneous analysis of relaxed and total mtDNA changes, it is plausible to suggest that the high dose of H_2O_2 converted most, if not all, supercoiled mtDNA into open-relaxed forms in LNCaP cells during the first 15 min of treatment. Further accumulation of DNA strand breaks due to either damage or repair intermediates could cause fragmentation of damaged

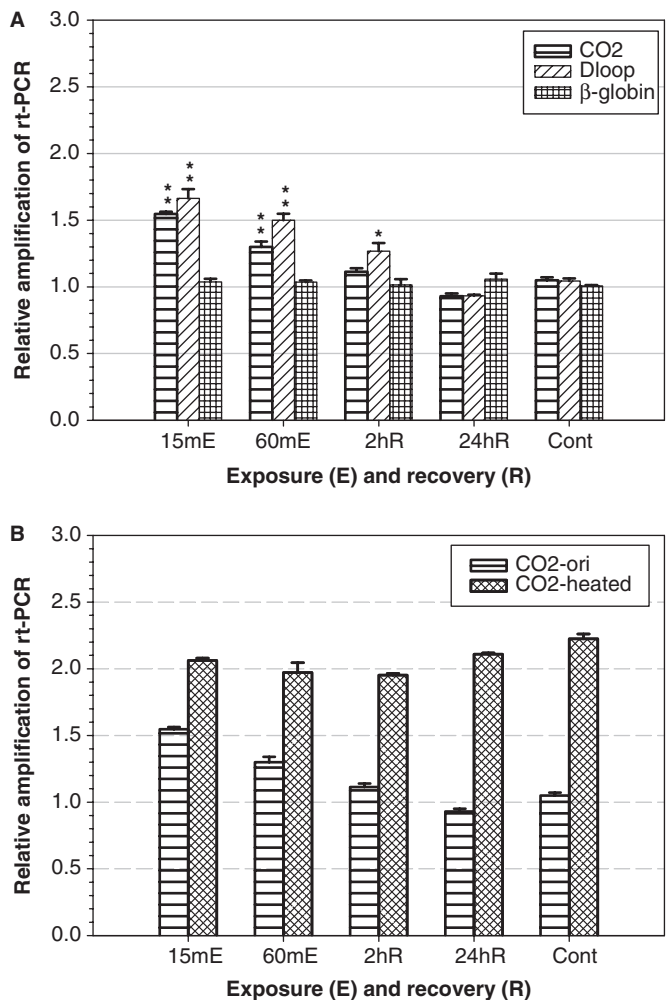


Figure 5. Structural damage and repair in mtDNA of LNCaP cells induced by $120 \mu M H_2O_2$ treatment. LNCaP cells ($2-2.5 \times 10^6$) that seeded 48 h before experiment were treated with $120 \mu M H_2O_2$ in serum-free medium for 15 and 60 min, respectively, to induce DNA damage. For recovery, LNCaP cells were first treated with $120 \mu M H_2O_2$ for 60 min, then allowed to recover in fresh complete medium for 2 and 24 h, respectively. (A) Structural damage and repair in mtDNA of LNCaP cells. Two mtDNA (CO2 and Dloop) and two nuclear DNA (β -actin and β -globin) markers were used for real-time PCR using total genomic DNA isolated from each sample. The relative amplification of each marker was expressed as in Equation 1 with β -actin gene from each template serving as a reference. (B) Quantification of total mtDNA content in LNCaP cells using heat-denatured DNA templates. Aliquots of total genomic DNA from each sample were heat-denatured at $95^\circ C$ for 6 min and then used for real-time PCR analysis using mtDNA marker CO2 (heated). The relative amplification of the marker was expressed as above with β -actin gene from each original template serving as a reference. Data from duplicate treatments were pooled and analyzed using the one-way analysis of variance in the Prism program (* $P < 0.05$; ** $P < 0.01$).

mtDNA molecules rather than repair, leading to near 2-fold reduction in total mtDNA content during the early recovery. Sustained reduction in mtDNA content was evident even after 24-h recovery. However, a slight increase in total mtDNA amplification after 24-h recovery could be explained by limited synthesis of nascent mtDNA molecules in slowly recovering cells. Consistent with high

levels of early structural damage and subsequent copy number reduction in mtDNA, long PCR analysis of the same samples revealed substantial and persistent reduction in the amplification of a 16.2-kb mtDNA fragment, while a 13.5-kb nuclear DNA exhibited little change in stressed prostate cancer cells (Figure 6C).

DISCUSSION

Real-time PCR is increasingly used for quantification of mtDNA copy number changes in clinical and toxicity studies: the implicit assumption of these studies has been that all mtDNA molecules are amplified with the same efficiency. However, extracted mtDNA consists of a mixture of supercoiled and relaxed (i.e. open circular and/or linear) forms that reflect functional and damaged fractions of mtDNA, respectively, in the cell. In this study, we demonstrated for the first time that the structural/conformational changes in mtDNA have profound influence on real-time PCR quantification. This influence was used for sensitive detection of structure-mediated mtDNA damage and repair, and for accurately measuring active mtDNA copy number changes in stressed prostate cancer cells.

The real-time PCR signal from supercoiled DNA is less than relaxed or linear conformations. Consequently, it must be used with care to quantify mtDNA or supercoiled plasmid and viral DNA. This new finding is supported by the observation that real-time PCR amplification is a function of changes in the relaxed rather than the supercoiled fraction of plasmid DNA digested with enzymes or treated with ferrous iron (Figures 1 and 2). Thus, real-time PCR is very sensitive to conformational changes from supercoiled to relaxed/linear form caused by DNA strand breaks (mainly single-strand breaks) both *in vitro* and in the cell. We reason that a random single-strand break incurs global structural disruption of supercoiled DNA by completely releasing its supercoiled turns and base tensions, leading to increased efficiency for primer binding and elongation. Moreover, the extent of structural damage in starting templates can be effectively detected as quantitative differences in threshold amplification between DNA templates. On the other hand, real-time PCR appears to be less sensitive to base lesions or accumulation of multiple DNA strand breaks in mtDNA. This may be due to base lesions having limited effect, if any, on superhelical structures; while more than one strand break does not produce additional structural consequences when analyzed using real-time PCR. For example, both open circular and linearized conformations resulted in the same level of maximum increase in real-time PCR amplification; while little change was observed in the linear form of nuclear DNA markers such as β -actin and β -globin DNA even though substantial damage was evident in such DNA as analyzed using long PCR assays (Figure 3). Therefore, we demonstrated that conformation transitions mediated by DNA strand breaks are the main basis for sensitive detection of relaxed/linear mtDNA using real-time PCR. However, detection of relaxed mtDNA alone provides little information on that of

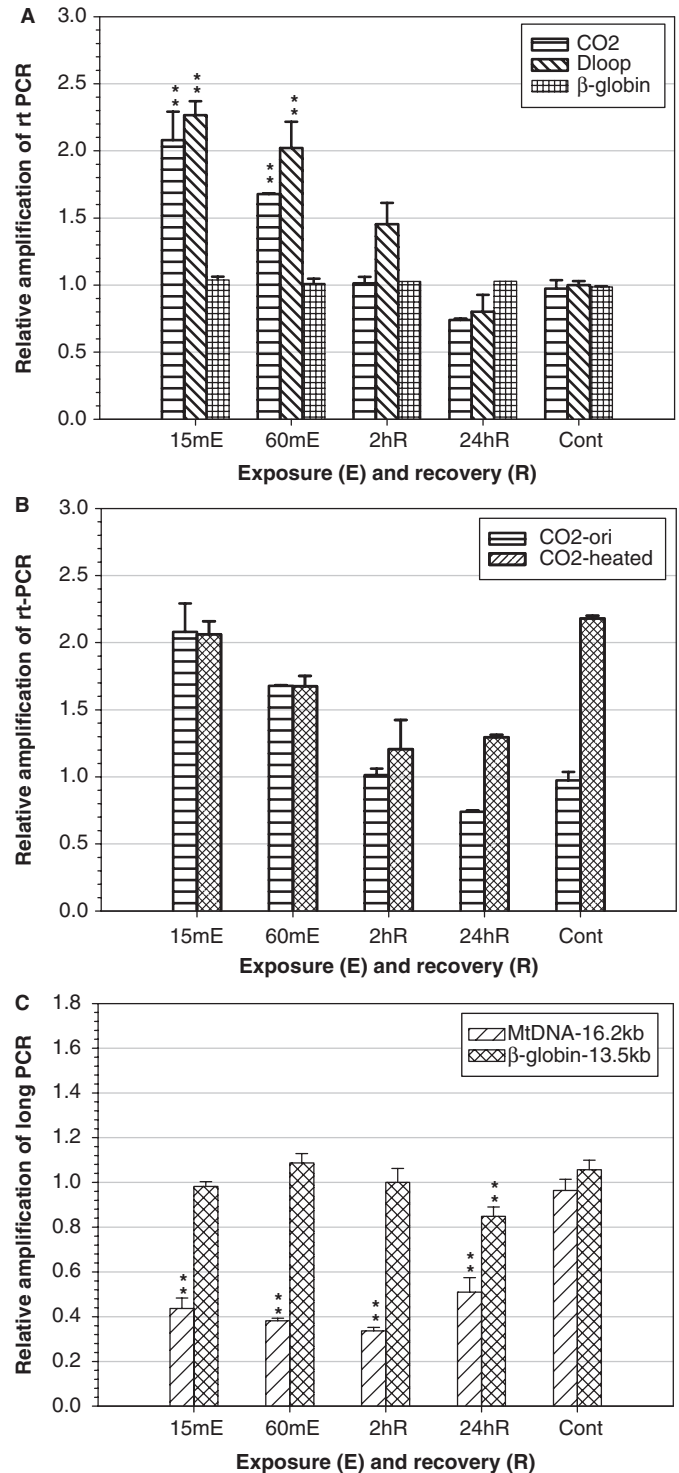


Figure 6. Structural damage and copy number reduction in mtDNA of LNCaP cells induced by 240 μ M H₂O₂ treatment. LNCaP cells were treated as in Figure 5 except that 240 μ M H₂O₂ was used for both exposure and recovery treatments. (A) Structural damage in mtDNA of LNCaP cells induced by 240 μ M H₂O₂. (B) Changes in total mtDNA content in LNCaP cells induced by 240 μ M H₂O₂. (C) Preferential mtDNA damage in LNCaP cells detected using long PCR. A 16.2-kb mtDNA and 13.5-kb β -globin DNA were amplified using long PCR to detect blocking lesions induced in both fragments. The relative amplification of each marker was expressed as A_D/A_O . Data from duplicate treatments were pooled and analyzed using the one-way analysis of variance in the Prism program (* $P < 0.05$; ** $P < 0.01$).

supercoiled and total mtDNA. A practical challenge to use real-time PCR in mtDNA analysis is the need to differentiate quantitative changes due to either copy number change or structural disruption. As demonstrated in the current study, heat-denaturation of template DNA appears to be an effective way of relaxing superhelical DNA by introducing single-strand breaks (Figure 4). The effect of heat-denaturation on structured DNA has dual implication in real-time PCR analysis. On one hand, it predicts that substantial single-strand breaks could be introduced into supercoiled DNA during real-time PCR reactions through repeated heat-denaturation steps with the initial step being most critical in determining the baseline levels of relaxed DNA. Therefore, it is essential to use 'hot-start' DNA polymerases that requires short initial time for heat-activation to maintain original proportions of different mtDNA fractions in template DNA. On the other hand, prolonged initial heat-denaturation provides a practical way of converting all superhelical DNA into its relaxed form, which allows subsequent quantification of total amount of mtDNA in a simple and effective fashion. Consequently, the superhelical fraction can be inferred from the quantitative differences between relaxed fraction and total mtDNA from the same templates. Thus, we propose that real-time PCR may serve as a sensitive new approach to detect different fractions of mtDNA both *in vitro* and in the cell.

Simultaneous detection of both relaxed fraction and total mtDNA content using real-time PCR provides a novel approach for quantitative analysis of induced mtDNA damage, repair and copy number change in human cancer cells. MtDNA is particularly sensitive to oxidative damage in both stressed cells and aging tissues (14–19); normal mitochondria possess a certain capacity to repair oxidative DNA damage through its base excision repair (BER) pathway (50,51), which is induced above normal levels by oxidative DNA damage (52). DNA strand breaks, especially single-strand breaks, are not only common lesions induced directly by ROS but also are key repair intermediates through which base lesions and abasic sites are repaired by the BER pathway, while accumulation of the lesions is cytotoxic (53). Thus, detection of this particular DNA lesion has broad implications in mtDNA damage, repair and functional consequences. Because DNA strand breaks cause a conformation transition from supercoiled to relaxed mtDNA, the accumulation or repair of strand breaks can be measured as an increase or decrease of the relaxed fraction of mtDNA, respectively. Real-time PCR, therefore, provides a new strategy for quantitative analysis of structure-mediated damage and repair in mtDNA by simultaneous detection of both relaxed and total mtDNA in stressed cells (Figure 7). As illustrated in the model, mtDNA exists as a mixture of supercoiled and relaxed/linear forms both in the cell and the extracted form (Figure 7A). The relaxed fraction represents the level of structural damage, and the difference between relaxed and total mtDNA reflects the portion of supercoiled DNA that is the functional form in the cell. Changes between three fractions of mtDNA can be used to infer induced structural damage, repair and copy number change using

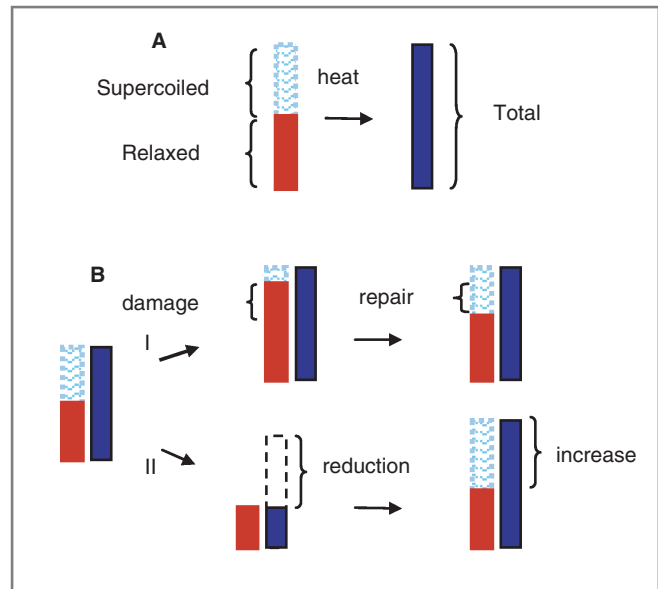


Figure 7. Model for simultaneous analysis of structural damage and repair as well as copy number change in stressed cells using real-time PCR. (A) Real-time PCR allows sensitive detection of relaxed (open circular/linear) or total mtDNA when all supercoiled DNA is converted into the relaxed forms using a heat-denaturation step. The ratio between relaxed and total mtDNA indicates the baseline levels of structural damage, while the quantitative differences between total and relaxed mtDNA represents the fraction of supercoiled DNA. (B) Induced structural damage and its subsequent repair can be detected by the increase or decrease of the relaxed fraction of mtDNA when total mtDNA content remains the same (I). However, quantitative changes in heat-denatured mtDNA indicate either reduction in mtDNA copy number due to fragmentation or increase due to nascent replication (II).

the same assay (Figure 7B). The strategy is not only validated in cell stress experiments using sub-lethal concentrations of hydrogen peroxide, but also reveals several surprising new findings in mtDNA responses to oxidative stress in prostate cancer cells. For example, a high base-line level of relaxed mtDNA as compared to total mtDNA (~40–50%) is observed in untreated control templates, likely reflecting high levels of spontaneous mtDNA damage in cultured prostate cancer cells. This feature holds the promise of being further exploited as a sensitive marker to physiological levels of oxidative damage in cancer cells and tissues. Meanwhile, structural damage in mtDNA was detected as a sensitive early response to oxidative stress, especially at low levels of stress, in prostate cancer cells. This was in contrast to the lack of sensitivity in detecting low levels of mtDNA damage using the long PCR assay. Moreover, high levels of oxidative stress could not only induce maximum levels of structural damage, but also trigger fragmentation of damaged molecules and sustained reduction in mtDNA content in prostate cancer cells. The long PCR assay, on the other hand, does not differentiate persistent damage in mtDNA due to either persistence of blocking lesions (i.e. strand breaks) or reduction in copy number. Thus, the real-time PCR approach reveals very dynamic mtDNA responses to oxidative stress in prostate cancer cells, which

involve not only structural damage and repair but also active copy number change under stressed conditions. These new findings are consistent with increased susceptibility of prostate cancer cells to oxidative stress and accelerated mitochondrial mutagenesis detected in clinical tissues (54–56). Further evidence to the dynamic mtDNA responses to oxidative stress and its biological implications in prostate malignancy are the subjects of intensive studies (Chen *et al.*, manuscript in preparation).

The real-time PCR strategy for the analysis of structure-mediated DNA damage and repair not only provides a new perspective to understand structural and functional consequences of oxidative damage in superhelical mtDNA, but may also find potential applications in the complex genomic DNA. This may be due to the extracted high-molecular-weight genomic DNA containing or mirroring the structural complexity of tens of thousands of genes and non-coding regions in the cell. Although nuclear DNA markers such as β -actin and β -globin exhibited little structural effect when analyzed using real-time PCR, it is conceivable that highly structured genomic loci such as repetitive genes, telomere and centromere regions, and many GC rich genes and regions may be potential candidates as structure-sensitive loci particularly susceptible to oxidative damage and other epigenetic modifications. Real-time PCR may provide a simple and effective approach for the scanning and characterization of such structural-sensitive loci in human chromosomes, whose structural changes may have broad implications in cancer development and progression (57,58).

ACKNOWLEDGEMENTS

We thank Dr G.P. Holmquist for useful discussion and critical reading of the manuscript. We also thank S. Chan for technical assistance; Drs A. Aprikian, S. Chevalier and M. Chevrette for their comments on earlier versions of the manuscript. Funding to pay the Open Access publication charge was provided by McGill University Health Centre Research Institute and McGill Prostate Cancer Centre of Excellence.

Conflict of interest statement. None declared.

REFERENCES

- Wallace,D.C. (2005) A mitochondrial paradigm of metabolic and degenerative diseases, aging, and cancer: a dawn for evolutionary medicine. *Annu. Rev. Genet.*, **39**, 359–407.
- Polyak,K., Li,Y., Zhu,H., Lengauer,C., Willson,J.K., Markowitz,S.D., Trush,M.A., Kinzler,K.W. and Vogelstein,B. (1998) Somatic mutations of the mitochondrial genome in human colorectal tumours. *Nat. Genet.*, **20**, 291–293.
- Penta,J.S., Johnson,F.M., Wachsmann,J.T. and Copeland,W.C. (2001) Mitochondrial DNA in human malignancy. *Mutat. Res.*, **488**, 119–133.
- Chen,J.Z. and Kadlubar,F.F. (2004) Mitochondrial mutagenesis and oxidative stress in human prostate cancer. *J. Environ. Sci. Health C. Environ.*, **22**, 1–12.
- Anderson,S., Bankier,A.T., Barrell,B.G., de Bruijn,M.H., Coulson,A.R., Drouin,J., Eperon,I.C., Nierlich,D.P., Roe,B.A. *et al.* (1981) Sequence and organization of the human mitochondrial genome. *Nature*, **290**, 457–465.
- Clayton,D.A. (2000) Transcription and replication of mitochondrial DNA. *Hum. Reprod.*, **15** (Suppl. 2) 11–17.
- Turrens,J.F. and Boveris,A. (1980) Generation of superoxide anion by the NADH dehydrogenase of bovine heart mitochondria. *Biochem. J.*, **191**, 421–427.
- Richter,C. (1995) Oxidative damage to mitochondrial DNA and its relationship to aging. *Int. J. Biochem. Cell Biol.*, **27**, 647–653.
- Toyokuni,S., Okamoto,K., Yodoi,J. and Hiai,H. (1995) Persistent oxidative stress in cancer. *FEBS Lett.*, **358**, 1–3.
- Herrmann,P.C., Gillespie,J.W., Charboneau,L., Bichsel,V.E., Pawelz,C.P., Calvert,V.S., Kohn,E.C., Emmert-Buck,M.R., Liotta,L.A. *et al.* (2003) Mitochondrial proteome: altered cytochrome c oxidase subunit levels in prostate cancer. *Proteomics*, **3**, 1801–1810.
- Fliss,M.S., Usadel,H., Caballero,O.L., Wu,L., Buta,M.R., Eleff,S.M., Jen,J. and Sidransky,D. (2000) Facile detection of mitochondrial DNA mutations in tumors and bodily fluids. *Science*, **287**, 2017–2019.
- Parrella,P., Xiao,Y., Fliss,M., Sanchez-Cespedes,M., Mazzarelli,P., Rinaldi,M., Nicol,T., Gabrielson,E., Cuomo,C. *et al.* (2001) Detection of mitochondrial DNA mutations in primary breast cancer and fine-needle aspirates. *Cancer Res.*, **61**, 7623–7626.
- Chen,J.Z., Gokden,N., Greene,G.F., Mukunyadzi,P. and Kadlubar,F.F. (2002) Extensive somatic mitochondrial mutations in primary prostate cancer using laser capture microdissection. *Cancer Res.*, **62**, 6470–6474.
- Richter,C., Park,J.W. and Ames,B.N. (1988) Normal oxidative damage to the mitochondrial and nuclear DNA is extensive. *Proc. Natl. Acad. Sci. USA*, **85**, 6465–6467.
- Mecocci,P., MacGarvey,U., Kaufman,A.E., Koontz,D., Schoffner,J.M., Wallace,D.C. and Beal,M.F. (1993) Oxidative damage to mitochondrial DNA shows marked age-dependent increases in human brain. *Ann. Neurol.*, **34**, 609–616.
- Hayakawa,M., Ogawa,T., Sugiyama,S., Tanaka,M. and Ozawa,T. (1991) Massive conversion of guanine to 8-hydroxy-guanosine in mouse liver mitochondrial DNA by administration of azidothymidine. *Biochem. Biophys. Res. Commun.*, **176**, 87–93.
- Ames,B.N., Shigenaga,M.K. and Hagen,T.M. (1993) Oxidants antioxidants and the degenerative diseases of aging. *Proc. Natl. Acad. Sci. USA*, **90**, 7915–7922.
- Yakes,F.M. and Van Houten,B. (1997) Mitochondrial DNA damage is more extensive and persists longer than nuclear DNA damage in human cells following oxidative stress. *Proc. Natl. Acad. Sci. USA*, **94**, 514–519.
- Santos,J.H., Hunakova,L., Chen,Y., Bortner,C. and Van Houten,B. (2003) Cell sorting experiments link persistent mitochondrial DNA damage with loss of mitochondrial membrane potential and apoptotic cell death. *J. Biol. Chem.*, **278**, 1728–1734.
- Radloff,R., Bauer,W. and Vinograd,J. (1967) A dye-buoyant-density method for the detection and isolation of closed circular duplex DNA: the closed circular DNA in HeLa cells. *Proc. Natl. Acad. Sci. USA*, **57**, 1514–1521.
- Robberson,D.L. and Clayton,D.A. (1972) Replication of mitochondrial DNA in mouse L cells and their thymidine kinase-derivatives: displacement replication on a covalently-closed circular template. *Proc. Natl. Acad. Sci. USA*, **69**, 3810–3814.
- Bogenhagen,D. and Clayton,D.A. (1978) Mechanism of mitochondrial DNA replication in mouse L-cells: introduction of superhelical turns into newly replicated molecules. *J. Mol. Biol.*, **119**, 69–81.
- Clayton,D.A. (1982) Replication of animal mitochondrial DNA. *Cell*, **28**, 693–705.
- Singh,G., Hauswirth,W.W., Ross,W.E. and Neims,A.H. (1985) A method for assessing damage to mitochondrial DNA caused by radiation and epichlorohydrin. *Mol. Pharmacol.*, **27**, 167–170.
- Lim,L.O. and Neims,A.H. (1987) Mitochondrial DNA damage by bleomycin. *Biochem. Pharmacol.*, **36**, 2769–2774.
- Hruszkewycz,A.M. (1988) Evidence for mitochondrial DNA damage by lipid peroxidation. *Biochem. Biophys. Res. Commun.*, **153**, 191–197.
- Itoh,H., Shioda,T., Matsura,T., Koyama,S., Nakanishi,T., Kajiyama,G. and Kawasaki,T. (1994) Iron ion induces mitochondrial DNA damage in HTC rat hepatoma cell culture—role of

- antioxidants in mitochondrial DNA protection from oxidative stresses. *Arch. Biochem. Biophys.*, **313**, 120–125.
28. Yaffee, M., Walter, P., Richter, C. and Muller, M. (1996) Direct observation of iron-induced conformational changes of mitochondrial DNA by high-resolution field-emission in-lens scanning electron microscopy. *Proc. Natl. Acad. Sci. USA*, **93**, 5341–5346.
 29. Asin, J., Perez-Martos, A., Fernandez-Silva, P., Montoya, J. and Andreu, A.L. (2000) Iron(II) induces changes in the conformation of mammalian mitochondrial DNA resulting in a reduction of its transcriptional rate. *FEBS Lett.*, **480**, 161–164.
 30. Walter, P.B., Knutson, M.D., Paler-Martinez, A., Lee, S., Xu, Y., Viteri, F.E. and Ames, B.N. (2002) Iron deficiency and iron excess damage mitochondria and mitochondrial DNA in rats. *Proc. Natl. Acad. Sci. USA*, **99**, 2264–2269.
 31. Santos, J.H., Mandavilli, B.S. and Van Houten, B. (2002) Measuring oxidative mtDNA damage and repair using quantitative PCR. *Methods Mol. Biol.*, **197**, 159–176.
 32. Higuchi, R., Fockler, C., Dollinger, G. and Watson, R. (1993) Kinetic PCR analysis: real-time monitoring of DNA amplification reactions. *Biotechnology (NY)*, **11**, 1026–1030.
 33. Heid, C.A., Stevens, J., Livak, K.J. and Williams, P.M. (1996) Real time quantitative PCR. *Genome Res.*, **6**, 986–994.
 34. Bustin, S.A. (2000) Absolute quantification of mRNA using real-time reverse transcription polymerase chain reaction assays. *J. Mol. Endocrinol.*, **25**, 169–193.
 35. Szuhai, K., Ouweland, J., Dirks, R., Lemaitre, M., Truffert, J., Janssen, G., Tanke, H., Holme, E., Maassen, J. *et al.* (2001) Simultaneous A8344G heteroplasmy and mitochondrial DNA copy number quantification in myoclonus epilepsy and ragged-red fibers (MERRF) syndrome by a multiplex molecular beacon based real-time fluorescence PCR. *Nucleic Acids Res.*, **29**, e13.
 36. Gahan, M.E., Miller, F., Lewin, S.R., Cherry, C.L., Hoy, J.F., Mijch, A., Rosenfeldt, F. and Wesselingh, S.L. (2001) Quantification of mitochondrial DNA in peripheral blood mononuclear cells and subcutaneous fat using real-time polymerase chain reaction. *J. Clin. Virol.*, **22**, 241–247.
 37. Cote, H.C., Brumme, Z.L., Craib, K.J., Alexander, C.S., Wynhoven, B., Ting, L., Wong, H., Harris, M., Harrigan, P.R. *et al.* (2002) Changes in mitochondrial DNA as a marker of nucleoside toxicity in HIV-infected patients. *N. Engl. J. Med.*, **346**, 811–820.
 38. von Wurmb-Schwark, N., Higuchi, R., Fenech, A.P., Elfstroem, C., Meissner, C., Oehmichen, M. and Cortopassi, G.A. (2002) Quantification of human mitochondrial DNA in a real time PCR. *Forensic Sci. Int.*, **126**, 34–39.
 39. Mambo, E., Gao, X., Cohen, Y., Guo, Z., Talalay, P. and Sidransky, D. (2003) Electrophile and oxidant damage of mitochondrial DNA leading to rapid evolution of homoplasmic mutations. *Proc. Natl. Acad. Sci. USA*, **100**, 1838–1843.
 40. Liu, C.S., Tsai, C.S., Kuo, C.L., Chen, H.W., Lii, C.K., Ma, Y.S. and Wei, Y.H. (2003) Oxidative stress-related alteration of the copy number of mitochondrial DNA in human leukocytes. *Free Radic. Res.*, **37**, 1307–1317.
 41. Ayala-Torres, S., Chen, Y., Svoboda, T., Rosenblatt, J. and Van Houten, B. (2000) Analysis of gene-specific DNA damage and repair using quantitative polymerase chain reaction. *Methods*, **22**, 135–147.
 42. Svoboda, P. and Harms-Ringdahl, M. (2002) Kinetics of phosphate-mediated oxidation of ferrous iron and formation of 8-oxo-2'-deoxyguanosine in solutions of free 2'-deoxyguanosine and calf thymus DNA. *Biochim. Biophys. Acta.*, **1571**, 45–54.
 43. Djuric, Z., Potter, D.W., Taffe, B.G. and Strasburg, G.M. (2001) Comparison of iron-catalyzed DNA and lipid oxidation. *J. Biochem. Mol. Toxicol.*, **15**, 114–119.
 44. Pfaffl, M.W., Horgan, G.W. and Dempfle, L. (2002) Relative expression software tool (REST) for group-wise comparison and statistical analysis of relative expression results in real-time PCR. *Nucleic Acids Res.*, **30**, e36.
 45. Pruss, G.J., Manes, S.H. and Drlica, K. (1982) Escherichia coli DNA topoisomerase I mutants: increased supercoiling is corrected by mutations near gyrase genes. *Cell*, **31**, 35–42.
 46. Pruss, G.J. (1985) DNA topoisomerase I mutants: increased heterogeneity in linking number and other replicon-dependent changes in DNA supercoiling. *J. Mol. Biol.*, **185**, 51–63.
 47. Schneider, J.E., Browning, M.M. and Floyd, R.A. (1988) Ascorbate/iron mediation of hydroxyl free radical damage to PBR322 plasmid DNA. *Free Radic. Biol. Med.*, **5**, 287–295.
 48. Rodriguez, H., Holmquist, G.P., D'Agostino, R. Jr., Keller, J. and Ackman, S.A. (1997) Metal ion-dependent hydrogen peroxide-induced DNA damage is more sequence specific than metal specific. *Cancer Res.*, **57**, 2394–2403.
 49. Kozyavkin, S.A., Pushkin, A.V., Eiserling, F.A., Stetter, K.O., Lake, J.A. and Slesarev, A.I. (1996) DNA enzymology above 100°C. *J. Biol. Chem.*, **270**, 13593–13595.
 50. LeDoux, S.P. and Wilson, G.L. (2001) Base excision repair of mitochondrial DNA damage in mammalian cells. *Prog. Nucleic Acid Res. Mol. Biol.*, **68**, 273–284.
 51. Mandavilli, B.S., Santos, J.H. and Van Houten, B. (2002) Mitochondrial DNA repair and aging. *Mutat. Res.*, **509**, 127–151.
 52. Driggers, W.J., Holmquist, G.P., LeDoux, S.P. and Wilson, G.L. (1997) Mapping frequencies of endogenous oxidative damage and the kinetic response to oxidative stress in a region of rat mtDNA. *Nucleic Acids Res.*, **25**, 4362–4369.
 53. Harrison, J.F., Hollensworth, S.B., Spitz, D.R., Copeland, W.C., Wilson, G.L. and LeDoux, S.P. (2005) Oxidative stress-induced apoptosis in neurons correlates with mitochondrial DNA base excision repair pathway imbalance. *Nucleic Acids Res.*, **33**, 4660–4671.
 54. Palapattu, G.S., Sutcliffe, S., Bastian, P.J., Platz, E.A., De Marzo, A.M., Isaacs, W.B. and Nelson, W.G. (2005) Prostate carcinogenesis and inflammation: emerging insights. *Carcinogenesis*, **26**, 1170–1181.
 55. Chen, J.Z., Gokden, N., Greene, G.F., Green, G. and Kadlubar, F.F. (2003) Simultaneous generation of multiple mitochondrial DNA mutations in human prostate tumors suggests mitochondrial hypermutagenesis. *Carcinogenesis*, **24**, 1481–1487.
 56. Parr, R.L., Dakubo, G.D., Crandall, K.A., Maki, J., Reguly, B., Aguirre, A., Wittock, R., Robinson, K., Alexander, J.S. *et al.* (2006) Somatic mitochondrial DNA mutations in prostate cancer and normal appearing adjacent glands in comparison to age-matched prostate samples without malignant histology. *J. Mol. Diagn.*, **8**, 312–319.
 57. Malins, D.C., Johnson, P.M., Barker, E.A., Polissar, N.L., Wheeler, T.M. and Anderson, K.M. (2003) Cancer-related changes in prostate DNA as men age and early identification of metastasis in primary prostate tumors. *Proc. Natl. Acad. Sci. USA*, **100**, 5401–5406. Epub 2003 Apr 17.
 58. Malins, D.C., Gilman, N.K., Green, V.M., Wheeler, T.M., Barker, E.A., Vinson, M.A., Sayeeduddin, M., Hellstrom, K.E. and Anderson, K.M. (2004) Metastatic cancer DNA phenotype identified in normal tissues surrounding metastasizing prostate carcinomas. *Proc. Natl. Acad. Sci. USA*, **101**, 11428–11431. Epub 2004 Jul 27.